EQUILIBRIUM, VISCOELASTICITY AND FRACTURE OF A SELF-ASSEMBLED TRANSIENT NETWORK MODEL

Christian Ligoure

LCVN UMR CNRS 5587, Université Montpellier 2
34095 Montpellier Cedex 05
France

The self-assembled transient networks constitute a class of complex materials forming spontaneously 3D networks at thermodynamical equilibrium, that can transmit transiently elastic stresses over macroscopic distances. These physical gels are generally formed of a network of polymer chains reversibly linked in a solvent. The transient nature of the junctions allow them, contrary to cross-linked networks, to relax the constraints by dissociation an reformation of the junctions: so they are able for instance to self-repair after dammage. Because of their spectacular viscoelastic properties, these materials have many applications . From the experimental results obtained with an experimental model this lecture will consider successively some general interesting physical properties for this class of of systems:(i) the pair potential induced by two beads reversibly linked by telechelic polymers, (ii), the phase behavior of the gels, (iii) the linear viscoelastic properties, and (iv) the nucleation and propagation of a fracture in this complex fluid.

Introduction

Transient self-assembling networks are common in both natural and synthetic materials. They consist of self-assembled aggregates (nodes) that are reversibly connected by links with a finite life-time as opposed to chemical gels where junctions are permanent. These physical gels exhibit two universal and independent features : a thermodynamic first order phase separation, which occurs at low volume fraction between a dilute and concentrated solution even in the absence of any specific interaction, and a non-thermodynamic topological transition, where an infinite network spanning the entire volume of the system is formed[.[1)] Telechelic polymers are often used as model linkers because they are architecturally simple: they consist of a long solvophilic midblock with each end terminated by a solvophobic short chain (a sticker). The stickers incorporate into the solvophobic domains of the aggregates and can bridge them via their solvent-soluble midblock resulting in an attractive interaction between the aggregates. The nature and the morphologies of the aggregates forming the network are versatile: (i) telechelic polymers in binary solution[2)] that self-assemble spontaneously into non interacting flowerlike micelles at low concentration and form three dimensional networks above a threshold concentration[3)] , (ii) surfactant vesicles[4)] , (iii) lyotropic lamellar phases[6)] (iv) wormlike micelles,[7)–9)] (v) spherical micelles,[10)] (vi) oil-in-water[11)] or water-in-oil[12)]microemulsion droplets.

This last system (telechelic-microemulsion mixtures) is of particular fundamental interest. Indeed, the advantage of this system is that the parameters that control the thermodynamics and structure of the physical gel can be easily identified and independently controlled: the concentration of nodes (the droplets) and the number

of polymers per droplets. This is in contrast with binary mixtures of telechelics, where the number of nodes formed by the associating chain ends and the number of links cannot be controlled separately. Other advantages of this system are the spherical symmetry which allows for instance a simple structural analysis in the Fourier space from scattering experiments and the versatility of the control of the surface curvature.

On the other side, linear rheological properties are very simple and have been indeed very well described by a simple Maxwell fluid model with a single relaxation time and a single zero shear modulus. Again the elastic modulus is easily controlled by the number density of polymer bridges in the sample whereas the relaxation time can be tuned by changing the chemical length of the stickers. Finally This system exhibit a very peculiar sudden rupture mode reminiscent of a brittle fracture in solid materials.[14)]

So, the telechelic -micromemulsion mixtures serve as an elegant model system for a general class of transient networks and allow to investigate both the equilibrium, structural, flow an fracture properties of transient networks. In this lecture, we will first describe the model system, and address successively (i) the pair potential induced by two beads reversibly linked by telechelic polymers, (ii), the phase behavior of the microemulsion-telechelics mixtures, (iii) the linear viscoelastic properties, and (iv) the nucleation and propagation of a fracture in this brittle fluid.

§1. Experimental system

The telechelics-microemulsion mixture system system is composed of an oil-in-water droplet microemulsion to which telechelic polymers are added . This system was previously described by Filali et al.[11)] The o/w microemulsion involves a cationic surfactant, cetyl-pyridinium chloride CPCl, and a cosurfactant n-octanol. The droplets are swollen with decane and dispersed in 0.2 M NaCl brine. The droplets are spheres of radius $b = 62$ $\mathring{A}$ and were found robust to variations of both the microemulsion concentration and of the amount of added polymer.[11)] The volume fraction in oil droplets is denoted ϕ. The polymer chains (Poly-ethylene oxide) of molecular weight 10 kDalton are grafted at both ends with aliphatic chains of eighteen CH_2 groups. This hydrophobic end groups (stickers) anchor reversibly into the microemulsion droplets. The polymer amount is represented by the connectivity r, i.e. the average number of hydrophobic stickers per droplet. The polymers chains can either link two oil droplets (bridge configuration) or loop one a single one (loop configuration). The other possible states (free chains with no stickers adsorbed into a sphere of dangling chains with a single sticker adsorbed) are negligible. Indeed, For aqueous transient networks, the stickers consist of short chains of typically 10-25 methylene groups, with a sticking energy on the order of kT per methylene group. Therefore,the corresponding sticking energy is $\epsilon/kT \approx 10 - 25$ is large enough to neglect the fraction of dangling or free chains.

The phase diagram[13)] is shown In Figure 2. For sufficiently low amount of telechelic polymers a one phase region is obtained for all volume fraction of droplets. For higher r, phase separation occurs in a wide range of droplets volume fraction. The

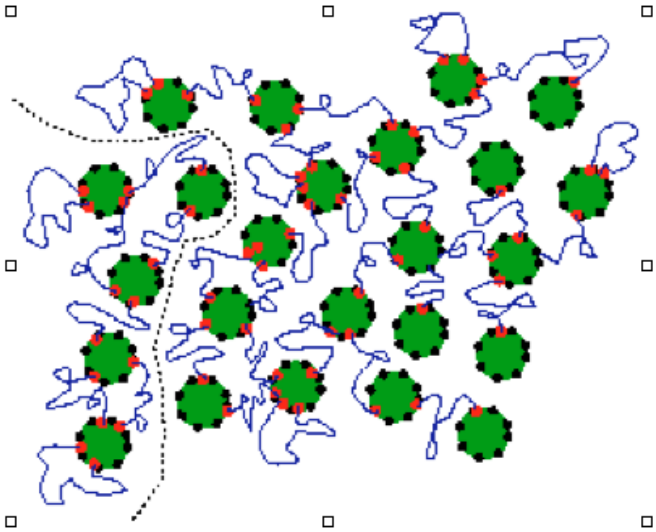

Fig. 1. Schematic of a bridged microemulsion. The telechelic polymers can either link two oil droplets or loop on a single one.

biphasic region comprises two isotropic and transparent phases, one being a rather stiff gel and the other being a fluid of low viscosity. In the one phase region, a sol-gel transition (this is a topological transition and not a thermodynamic transition) and defined the percolation line. A generic phase behavior is expected for mixed systems of self-assembled aggregates and polymeric crosslinkers: an entropically driven, first-order thermodynamic phase transition is predicted to occur even in the absence of any specific interactions at the mean-field level.[1)] The configurational entropy of polymer junctions induces indeed an effective attraction that can result in an equilibrium between a dilute phase and a connected network.

§2. Pair potential between two droplets induced by telechelic polymers[15)]

Let consider two spheres of diameter σ separated by a distance h than interact through ideal telechelic polymer chains of N monomers of size a. The polymers are in contact with a bulk reservoir of chemical potential μ. The stickers are free to diffuse onto the spheres and the sticking energy $\epsilon \gg kT$, so that the free chain configurations and the dangling chains configurations are negligible. We first consider the simpler case of two infinite walls separated by a distance h along the z axis.it consists of M sites of area a^2 which can be either occupied by a surfactant molecule or by the sticker of a telechelic polymer of polymerization index N. The statistical weight associated with all configurations of an ideal chain of N monomers located between the two impenetrable walls with its first monomer at $\mathbf{r} = (x, y, z)$ and its last one at $\mathbf{r}' = (x', y', z')$ is given by the chain propagator equation:[16)]

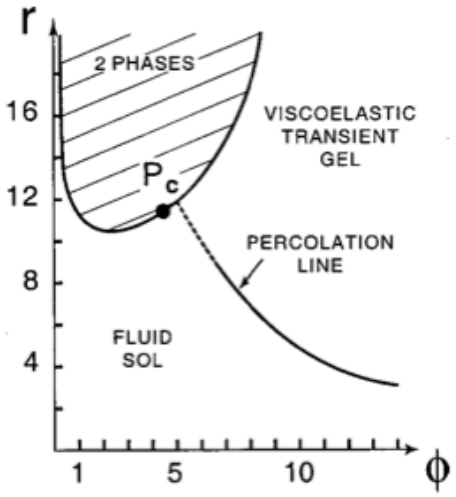

Fig. 2. Phase diagram of the connected microemulsion a a function of the droplet volume fraction ϕ and the mean number of polymer stickers per droplet r.

$$\Big(\frac{\partial}{\partial N} - \frac{a^2}{6}\nabla^2\Big)G_N(\mathbf{r},\mathbf{r}') = 0 \tag{2·1}$$

where $G_N(\mathbf{r},\mathbf{r}') = 0$ outside the space between the walls.

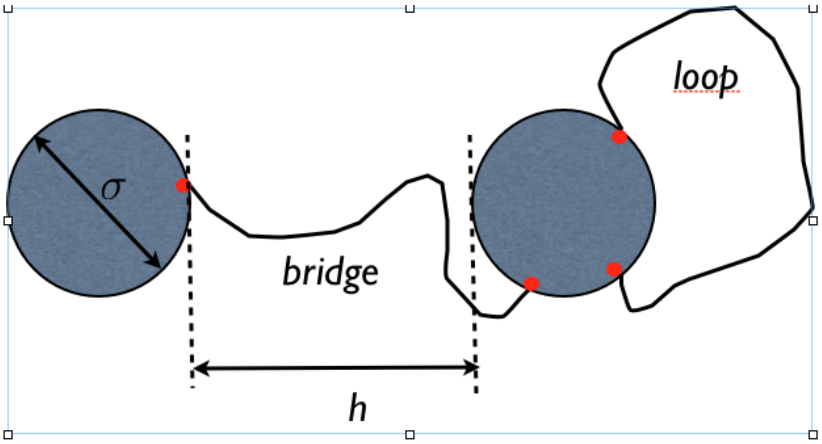

Fig. 3. Two beads interacting via a telechelic polymer

The solution of Eq.(2·1)is given by standard methods:

$$G_N(\mathbf{r},\mathbf{r}') = \frac{3}{2\pi N a^2}\exp\Big[-\frac{3}{2Na^2}[(x-x')^2+(y-y')^2)\Big]\times\frac{2}{h}\sum_{p=1}^{\infty}\exp\Big[\frac{-\pi^2 N a^2}{6h^2}p^2\Big]\sin\frac{\pi p z}{h}\sin\frac{\pi p z'}{h} \tag{2·2}$$

A loop configuration is obtained by demanding that $\mathbf{r_0} = (0, 0, a)$ and $\mathbf{r'_0} = (x', y', a)$ and the corresponding loop partition function is:

$$z_l(h) = a \int_{-\infty}^{+\infty} dx' \int_{-\infty}^{+\infty} dy' G_N(\mathbf{r_0}, \mathbf{r'}) = \frac{2a}{h} \sum_{p=1}^{\infty} e^{-\frac{\pi^2 N a^2}{6h^2} p^2} \sin^2 \frac{p\pi a}{h} \tag{2·3}$$

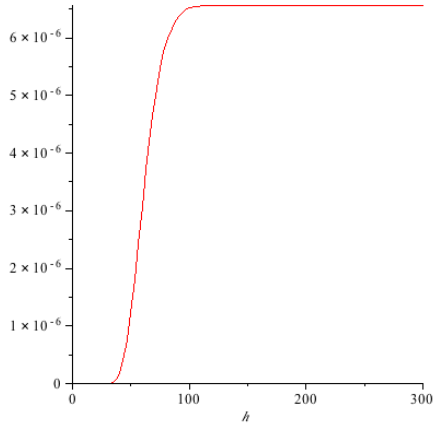

Fig. 4. Partition function of a loop (Eq. 2·3)

A bridge configuration is obtained by demanding that $\mathbf{r_0} = (0, 0, a)$ and $\mathbf{r'_0} = (x', y', h - a)$ and the corresponding bridge partition function is then:

$$z_b(h) = a \int_{-\infty}^{+\infty} dx' \int_{-\infty}^{+\infty} dy' G_N(\mathbf{r_0}, \mathbf{r'}) = \frac{2a}{h} \sum_{p=1}^{\infty} (-1)^{p+1} e^{-\frac{\pi^2 N a^2}{6h^2} p^2} \sin^2 \frac{p\pi a}{h} \tag{2·4}$$

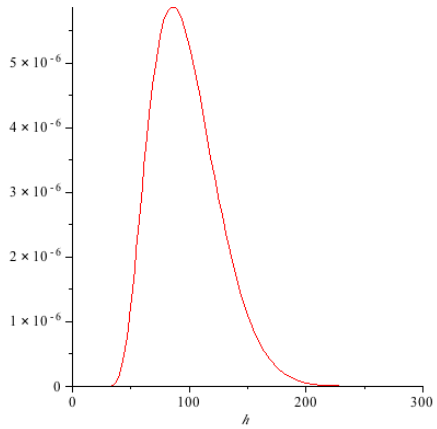

Fig. 5. Partition function of a bridge (Eq. 2·4)

From Eqs(2·3,2·4) one gets:

$$z_l(\infty) = \frac{3\sqrt{6}}{n^{3/2}} \tag{2·5}$$

$$z_b(\infty) = 0 \tag{2·6}$$

As expected the bridge partition function vanishes if the two wall are far apart($h \to \infty$), whereas the loop partition function remains constant. Ideal chains by hypothesis do not interact, so, the partition function of Q ideal chains sticked on a pair of wall is:

$$Z_Q(h) = \binom{Q}{M} (z_b(h) + z_l(h))^Q \tag{2·7}$$

The corresponding grand partition function reads:

$$\Xi(h) = \sum_{Q=0}^{M} Z_Q(h) e^{\beta\mu Q} \tag{2·8}$$

where μ is the chemical function of a polymer chain. Note that we use the grand canonical statistical ensemble, because chains are free to exchange with the bulk reservoir. The grand potential *per unit area* is:

$$J(h) = \frac{kT}{a^2} \ln[1 + e^{\beta\mu}(z_b(h) + z_l(h))] \tag{2·9}$$

where z_l and z_b arge given by Eqs (2·3,2·4).

The polymer-induced effective potential per unit area between the two walls is then:

$$V(h) = J(h) - J(\infty) = -\frac{kT}{a^2} \ln \frac{1 + e^{\beta\mu} z(h)}{1 + 3\sqrt{6} N^{-3/2} e^{\beta\mu}} \tag{2·10}$$

where:

$$z(h) = z_l(h) + z_b(h) = \frac{4a}{h} \sum_{p=0}^{\infty} e^{-\frac{\pi^2 N a^2}{6h^2}(2p+1)^2} \sin^2 \frac{(2p+1)\pi a}{h} \tag{2·11}$$

One has to keep in mind that the mean number of adsorbed polymer per unit area $\langle q(h) \rangle = -\partial J/\partial\mu$ is *not* a conserved quantity, that is depends on h. So, in the biphasic domain of the phase diagram, there is no reason that droplets in the dilute phase bear the same mean number of polymers than droplets in the gel phase.

The effective pair potential induced by telechelic polymers $V(h)$ is plotted in Fig.(6). It exhibits an attractive minimum for a distance between the walls on the order of the end to end distance of a polymer chain $R = aN^{1/2}$; for this distance, the fraction of bridges is maximal. At larger distances, there is an entropic penalty for the bridge configurations because bridges must be stretched. At shorter distance the entropic cost of polymer confinement (for both loops and bridges configurations) induces an effective repulsion between the walls.

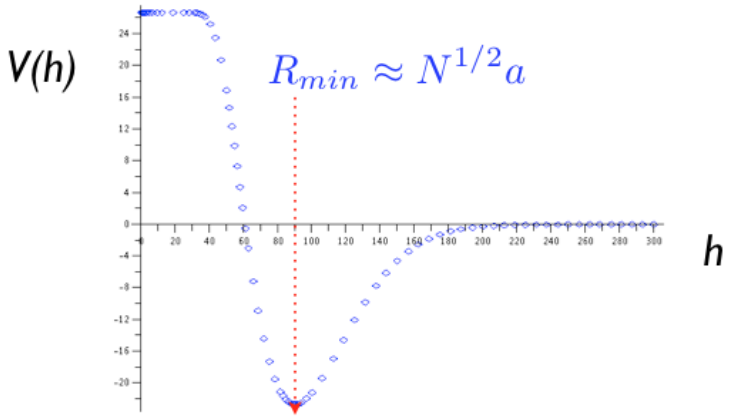

Fig. 6. Polymer induced effective potential per unit area between two walls

To extend these results to curved surfaces, we use the Derjaguin approximation despite the fact that the curvature of the droplets are of the same order of magnitude than the size of polymer chain.The Derjaguin approximation[17] is a powerful approximation widely use in colloidal science which gives the force between two spheres in terms of the energy per unit area of two flat surfaces at the same separation it is applicable to any type of force law, whether attractive, repulsive or oscillatory, so long as the range of the interaction and the separation is much less than the radii of the spheres . Finally on obtains the contribution $V_p(h)$ of the polymer to the interaction potential between the droplets of diameter σ at distance h from Eqs.(2·10,2·11):

$$V_p(h) = \frac{\pi\sigma}{2}\int_{\infty}^{h} V(h')dh' \qquad (2\cdot12)$$

The potential V_p is plotted in Figure(7)

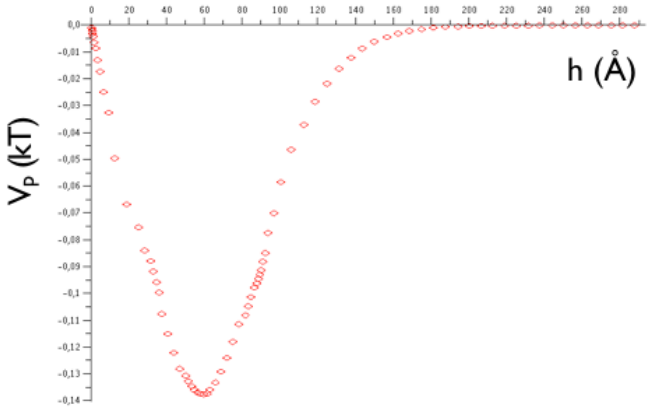

Fig. 7. Polymer induced effective potential per unit area between two spheres (**??**)

The attractive minimum for a distance between spheres on the order of the

polymer end to end distance is still present. However the repulsion at short distances disappears. this a consequence of the fact , that, even at close contact, a bridge or a loop can exist because the stickers freely slide onto the spheres as shown by Monte Carlo simulations;[18] For real chains, where the potential is non additive with the mean number of polymer/per bead, the simulations show the repulsion due to the entropic confinement of the polymer chains. The effective potential V_p has been tested to fit the small angle neutron scattering data for the structure factor of the experimental system:[15] the agreement is qualitative; however, the potential underestimates the repulsion between the spheres, due to the sliding effect , which become less and less important for the $N > 2$ bodies contributions to the potential between spheres.

§3. Entropic phase separation in polymer-microemulsions network[19]

A simple mean-field theory has been developed by Zilman *et al*[19] to explain the experimental phase digram shown in Fig.2. It predicts how the polymer properties control the phase behavior. The predicted phase separation has a *purely entropic origin*: there are no energetic interactions among the polymers or droplets. The phase separation occurs because the loss of the translational entropy of the droplets is overcompensated by the high configurational entropy of the polymer connections in the dense network.

A total of N_p polymers and $\mathcal{N}$ beads are distributed in space so that a polymer either connects two beads or loops on a single bead. The total free energy of the systems which is athermal amounts to the configurational entropy. The first term is the translation entropy of mixing of a dispersion of hard spheres given in lattice representation by:

$$S_0 = -k[\phi \ln \phi + (1-\phi)\ln(1-\phi)] \tag{3·1}$$

where $S_0(\phi)$ is the entropy per site on the lattice and ϕ is the volume fraction of the beads.

The second contribution is the configurational entropy of distributing the polymers among the beads.

For a single polymer there are $q_l\mathcal{N}$ available looped states where q_l is the number of positions available to a sticker of size a at the surface of a drop: $q_l \simeq \sigma^2/a^2$ (σ is the diameter of a bead). The free energy cost ϵ_l (in kT units) of a looped polymer measures the entropic cost of both ends being confined to the same droplet. In a simple approximation, the number of configurations available to a polymer with radius R_G, and with both ends constrained to a volume v, that is small relative to the total volume is proportional to $(v/R_G^3) \simeq \sigma^2 l/R_G^3)$ where l is the length of the hydrophobic sticker. Therefore $e^{-\epsilon_l} \simeq (\sigma^2 l/R_G^3)$ for $\sigma < 2R_G$ and saturates to unity for $\sigma > 2R_G$.

We calculate now the mean number of beads connected by a polymer. For a bead located a the origine O, the mean number of droplets at a distance $[R, R+dR]$ is $\frac{4\pi R^2 dR\phi}{\pi\sigma^3/6}$. This gives the number of pair droplets at a distance $[R, R+dR]$ $(R > \sigma)$

$$\frac{\mathcal{N}}{2}\frac{4\pi R^2 dR\phi}{\pi\sigma^3/6} = q(R)dR \tag{3·2}$$

A bridge connecting two beads at distance R has stretching energy on the order of $E_R = \frac{3}{2}kTR^2/(Na^2)$.

The partition function of a single chain is:

$$Z_1 = q_l\mathcal{N}e^{-\epsilon_l} + \int_{\sigma/2}^{\infty} q(R)e^{-E(R)/(kT)}dR = q_l\mathcal{N}e^{-\epsilon_l} + q\phi\mathcal{N} \tag{3·3}$$

with

$$q = \int_{\sigma/2}^{\infty} \frac{24R^2}{\sigma^3}\exp\left(-\frac{3}{2}\frac{R^2}{Na^2}\right)dR \tag{3·4}$$

The partition function of N_p chains which are undistinguishable and independent is:

$$Z_p = \frac{1}{N_p!}Z_1^{N_p} = \frac{(q_l\mathcal{N}e^{-\epsilon_l} + q\phi\mathcal{N})^{N_p}}{N_p!} \tag{3·5}$$

The free energy per lattice site of the system is $f = -kT/V(lnZ_p - TS_0(\phi))$. From Eqs.(3·1, 3·5) with $c = N_p/V$ and $\phi = \mathcal{N}/V$ one gets:

$$\frac{f(\phi,c)}{kT} = \phi\ln\phi + (1-\phi)\ln(1-\phi) + c(\ln c - 1) - c\ln(q\phi^2 + \phi q_l e^{-\epsilon_l}) \tag{3·6}$$

The first and second terms in Eq.(3·6) corresponds to the translational entropy of the droplets; the third term corresponds the translational entropy of the polymers, and the last term describes the effective interaction between the droplets and the polymers.

The mixed system is stable if $f(\phi,c)$ is a convex function, i.e $\delta^2 f = f_{\phi\phi}\delta\phi^2 + 2f_{\phi c}\delta\phi\delta c + f_{cc}\delta c^2$ should be a positive bilinear form. So, the matrix

$$\mathbf{S} = \begin{pmatrix} f_{\phi\phi} & f_{\phi c} \\ f_{\phi c} & f_{cc} \end{pmatrix}$$

must have two positive eigenvalues. Simple algebraic manipulations show that f_{cc} is positive , so the condition of stability reduces to $\det\mathbf{S} > 0$, i.e.:

$$2\frac{c}{\phi} < \frac{\phi + (q_l/q)e^{-\epsilon_l}}{\phi(1-\phi)} \tag{3·7}$$

The mean number of stickers per bead is $r = 2c/\phi$, so the spinodal is defined by

$$r = r_s = \frac{\phi + (q_l/q)e^{-\epsilon_l}}{\phi(1-\phi)} \tag{3·8}$$

Eq.(3·8) defines the spinodal line in the plane (ϕ, r) ,i.e., if $r > r_s$, the system is thermodynamically unstable and phase separates into a system of dense droplets that are highly connected by polymers, that coexists with a dilute system of almost

disconnected droplets, decorated with polymer loops. The latter observation stems from the fact that the average fraction of the looped polymers $\overline{\lambda}$ is given by:

$$\overline{\lambda} = \frac{-\partial \ln Z_1}{\partial \epsilon_l} = \frac{(q_l/q)\exp(-\epsilon_l)}{(q_l/q)\exp(-\epsilon_l) + \phi} \tag{3·9}$$

In the dilute phase $\phi \to 0$ and $\overline{\lambda} \to 1$

In the coexistence phase domain, the equality of f the polymer chemical potentials $\mu_c = \partial f/\partial c$ in the two coexisting phases implies that:

$$r = m\left(\phi + \frac{q_l}{q}e^{-\epsilon_l}\right) \tag{3·10}$$

where m is a constant defined by $m = \frac{2e^{\mu_c}}{q}$. It follows that the coexisting phases lie along the lines given by Eq.(3·10), which are *not* horizontal in the (ϕ, r) plane.

Inersection points of the coexisting lines Eq(3·10) and the spinodal Eq.(3·8) are the solutions of the equation $\phi^2 - \phi + m = 0$. For $m < 4$ there is no solution , and so no phase coexistence. For $m = 4$, there is a single solution $(\phi = 0.5; r = r_c = 2 + 2\frac{q_l}{q}e^{-\epsilon_l})$ which defines the critical point that is *not* the minimum of the spinodal. For $m > 4$ there are two solutions (be careful that these solutions do not define the binodal). These simple analytical results reproduce qualitatively well the phase behavior of the experimental system and are summarized in Figure 8. Computer simulations of the same system[20] verify the predictions of the analytical model.

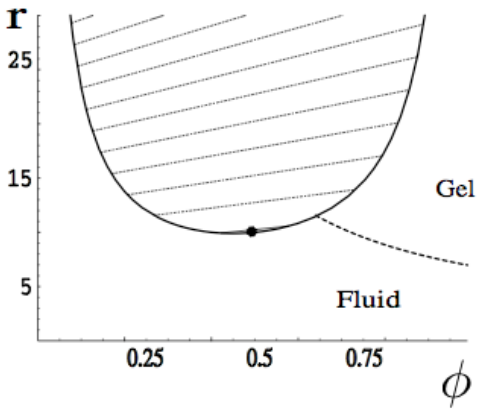

Fig. 8. Phase diagram[19] of drops connected with polymers. The thick line is the spinodal line of the phase separation for $q_l e^{-\epsilon_l}/q = 2$. Above this line the system becomes thermodynamically unstable. The critical point is at$\phi = 0.5$ and is shown as a black dot. Note that the critical point is not at the minimum of the spinodal. The tie lines are shown as dotted lines in the phase separation region. Note that they are not horizontal. The dashed line shows the percolation threshold calculated for an fcc lattice with $q = 16$. Below the percolation line, the system is in the fluid state, while above it a connected gel is formed

Because of its entropic nature, the phase separation is extremely robust and is independent of the detailed as-sumptions about the polymer an/or the nodes

properties. For instance its is also predicted using a self consistent field theory for binary solutions of telechelic chains[21] in agreement with experimental results,[22].[23] The same type of phase separation has been also observed with entangled solutions of wormlike micelles bridged by telechelic polymers.[7]

§4. Linear viscoelastic properties

Th gel phase of the bridged microemulsion behaves as a Maxwell, fluid, that is the simplest viscoelastic behavior: the material can be characterized by a single plateau shear modulus μ_0 and a single relaxation time τ. The constitutive differential scalar equation of a Maxwell fluid is obtained from the spring and dashpot representation of a Maxwell element (Fig. 9).

$$\sigma + \tau \frac{d\sigma}{dt} = \eta \frac{d\gamma}{dt} \tag{4·1}$$

where σ is the shear stress, γ is the shear strain and $\eta = \mu_0 \tau$ is the viscosity of the Maxwell fluid.

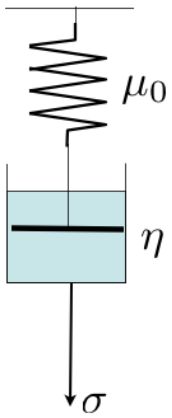

Fig. 9. Spring and dashpot representation of a Maxwell element

When a Maxwell fluid is submitted to an oscillatory stress at frequency ω characterized by its complex form $\underline{\sigma} = \sigma_0 \exp i\omega t$ the material response given by the complex strain $\underline{\gamma}$ is of the form $\underline{\sigma} = \underline{\mu}(\omega)\underline{\gamma}$.

$Re(\underline{\mu}(\omega)) = \mu'(\omega))$defines the storage modulus of the material and $Im(\underline{\mu}(\omega) = \mu''(\omega)$ is the loss modulus. From Eq. 4·1, one gets the storage and loss moduli for a Maxwell fluid:

$$\mu'(\omega) = \mu_0 \frac{(\tau\omega)^2}{1 + (\tau\omega)^2} \tag{4·2}$$

$$\mu''(\omega) = \mu_0 \frac{\tau\omega}{1 + (\tau\omega)^2} \tag{4·3}$$

At low frequency ($\omega\tau \ll 1$), the modulus is purely imaginary ($\mu = i\omega\mu_0\tau$) and

the material behaves as a liquid of viscosity $\eta = \mu_0\tau$. At high frequency ($\omega\tau \gg 1$) we are dealing with an elastic solid with an elastic moculus $\mu \approx \mu_0$.

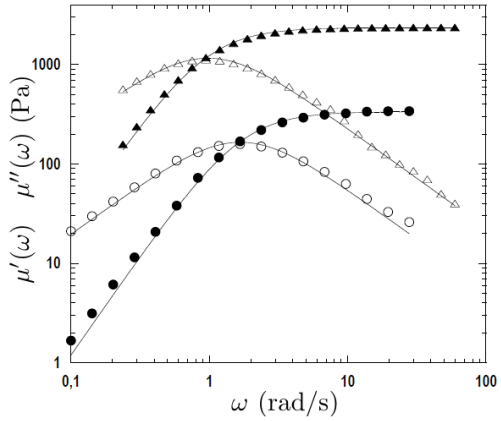

Fig. 10. Frequency sweep experiments. Storage modulus, μ' (closed symbols) and loss modulus, μ" (opened symbols) as a function of the frequency ω for the fluids $[r = 6, \phi = 10\%]$ (circles) and $[r = 12, \phi = 10\%]$ (triangles). Solid lines correspond to fits by a Maxwell mode (Eqs. 4·2, 4·3) which give the elastic shear modulus and the relaxation time of each fluid.

Figure 10 show that the Maxwell behavior is almost perfect for the telechelics-microemulsion mixtures. The shear modulus and the relaxation time are respectively equal to 330 Pa and 0.59 s for $[r = 6, \phi = 10\%]$, 2400 Pa and 2 s for $[r = 12, \phi = 10\%]$.[24)]

The origin of the Maxwell behavior is explained by the transient network theory.[25)] We summarize here the main results. At high frequency, where we can neglect the transient nature of the network the gel is a a polymer network. The simplest model to describe the elastic properties of a permanent polymer network like a rubber is the affine network model which is described in textbooks (see for instance Ref.[27)]). The elasticity arises primarily from the changes in entropy of the network strands when the network is macroscopically deformed. So the shear modulus is:

$$\mu_0 = n_b kT \tag{4·4}$$

where $n_b \propto \frac{r}{2}\phi$ is the number density of polymer bridges. The stress relaxation arises from the finite residence time τ_R of a sticker in a given droplet. Since the escape of a given sticker from a droplet is presumably a thermally activated process, we expect τ_R and therefore $\tau \propto \tau_R$ to exhibit an Arrhenius dependance versus the temperature:

$$\tau = \tau_0 \exp(E_s/kT) \tag{4·5}$$

where τ_0 is some inverse frequency of attempts and the activation energy E_s is the reversible work of extraction of the sticker from the hydrophobic core into the free water. The activation energy is itself proportional to the number of methyl groups n_{CH_2} in a sticker $E \simeq 1.2kTn_{CH_2}$. The longer are the stickers of the telechelic chains, the longer is the relaxation time of the network. Eqs (4·4,4·5) do not describe

properly the viscoelastic behavior near the percolation line as shown in Figure 11. For a given droplet concentrations both the elastic plateau modulus and the relaxation time exhibit a power law dependance with the apparent connectivity r on the form $\mu_0(r) = A(r - r_p)^\alpha$ and $\tau = B(r - r_p)^\beta$, where r_p defines the percolation point of the network for a given ϕ.[28] In principle, in percolation situations, the singular power law dominates the evolution of a given quantity only close to the threshold. Far above, the mean field behavior is usually recovered. In contrast,in this system, the fits happen to be surprisingly good even far above $r_p(\phi)$ a feature that is not understood.

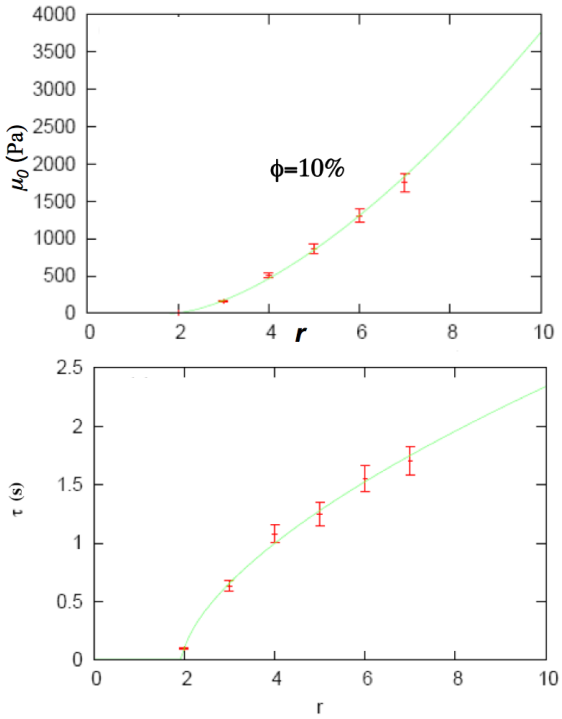

Fig. 11. Evolution of the shear modulus μ_0 and the relaxation time τ near the percolation threshold (Note that in these experiments the polymer chains have a molecular weight of 35kDa). The lines are t fits with the expressions $\mu_0(\text{Pa}) = 389(r - 1.9)^{1.55}$ and $\tau(\text{s}) = 0.6(r - 1.9)^{0.6}$

.

μ_0 characterizes the immediate elastic response of the network to a sudden deformation, before any relaxation due to the finite lifetime of a link. It is natural in this picture that it vanishes below a finite value r_p of the connectivity parameter: below r_p, there is no cross-linked infinite path, connecting continuously the cone and the plate of the rheometer and capable of sustaining the transient elastic torque. Since by definition μ_0 does not involve any feature related to relaxations, its evolution can be compared to theoretical predictions derived at true sol- gel transitions The exponent calculated for the elastic modulus is 1.7 above the gel point[29] close to the value measured in this system. The terminal relaxation time τ is related to the residence time of a sticker in a droplet. In the usual interpretation of the stress

relaxation in transient net- works[25),26)] the spatial distribution of the nodes is assumed to be affinely deformed by the step strain and the length distribution of the links is thus shifted accordingly. The transient off equilibrium length distribution is at the origin o f the measured stress . From time to time stretched links disengage due to the finite residence time of their stickers and reconnect with the equilibrium length distribution: they forget the initially imposed strain and no more contribute to the stress. In this picture the stress at time t is a simple measure of the number of links that still reminds the initial strain after time t, and we would expect τ to be simply identical to the residence time. The measurements do not support this expectation: τ sensitively depends on the average degree of connectivity r and vanishes at r_p, whereas the residence time is completely determined by the adsorption energy of a sticker in a droplet. It should not depend on nonlocal features such as the degree of connectivity of the network. To understand the discrepancy, we note that the above affine picture is a mean field description which assumes that the imposed strain distributes homogeneously within the network. Such homogeneity certainly breaks when approaching the percolation point. Close to the threshold, the infinite connected cluster consists of more densely cross-linked subclusters connected to each other by weaker parts where the links are less dense. Breaking a small number of links only, in a weak part, will suddenly release the stress within the whole adjacent dense subclusters. In this non-mean-field picture, we expect τ to be shorter than the residence time and indeed to vanish at the percolation as observed in the experiments.

§5. Microscopic mechanisms of the brittleness of the transient network[14)]

Her we investiigate the fracture nucleation in the transient network; indeed we will show that this liquid i liable to fracture in a brittle manner since it possesses structure capable of transmitting elastic forces over macroscopic scales. But this structure is also be labile and reversible to let the material flows; so the fracture should only be observed for high rates of deformation for which the fluid cannot relax, the material responding in a solid-like manner.

5.1. *Pendant drop experiments*

Such a brittle fracture can be observed for several flow geometries. we focus in this lecture on purely extensional flow experiments during a pendant drop experiment monitored with a fast camera , equipped with a macro lens, (Fig. 12). A syringe pump was used to form the drops with a fixed volume of 50 μL and a constant rate of 2 mL/h for all the solutions. The fluid initially in the syringe flows through a lower plastic tube of diameter of 2.60 mm and a drop emerges at the tube outlet which is enclosed in a glass box to reduce air currents.

During the experiment, the tensile stress steadily increases as the cylindrical body of the drop thins up. At any time, the recorded extension rate $\dot{\epsilon}$ as a function of the effective extensional stress σ_N agrees with the Maxwell model: the extensional viscosity at moderate rate is found three time larger than the shear viscosity ($\sigma_N \simeq$

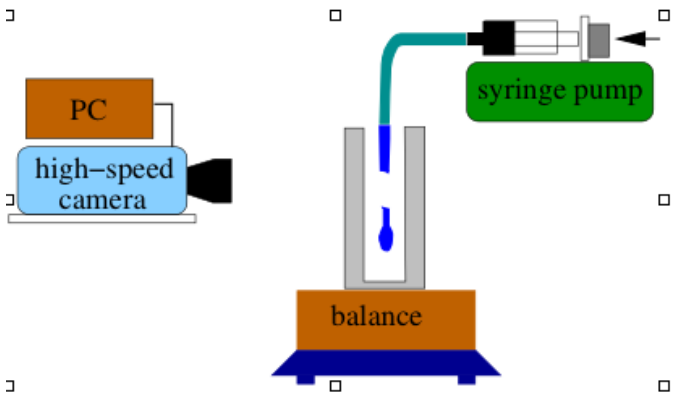

Fig. 12. Experimental setup for fracture observation in pendant drop experiments

.

$3\mu_0\tau\dot{\epsilon}$). But suddenly again, inside the linear regime ($\dot{\epsilon}\tau \simeq 0.2$), a fracture nucleates and propagates across the sample which leads to the rupture of the drop . We get the critical stress at the rupture of the drop σ_N in the following way. We measure the diameter of the drop where the fracture occurs and we weight the mass of the falling part with the help of a laboratory balance of accuracy 1 mg (placed underneath the injection set-up. In this condition the stress σ_{zz} is measured with a precision of 5%. Finally the stress at the rupture is equal to $\sigma_N = \sigma_{zz} - \sigma_{yy}$ with σ_{yy} the radial stress corresponding to the Laplace pressure. The failure is brief and completed within 20ms, which gives a crack speed of 25 mm/s, much slower than the transverse shear wave velocity ($\sqrt{\mu_0/\rho} \sim 1000mm/s$, with ρ the mass density of the fluid) (see Fig.13). It is worth noting that upon growing, the fracture exhibits the parabolic shape (Fig. 14) expected for an elastic solid breaking under tension.[30),31)]

When the polymer concentration changes (r increases) at fixed volume fraction of surfactant ($\phi = 10\%$), the critical fracture stress changes too as seen in Fig.15. Finally we observe that the critical rupture stress is independent of the sticking energy ϵ. Indeed experiments where performed with samples with the same polymer and surfactant concentration, but which differ by the length of the hydrophobic stickers (21 respectively 18 methyl group per sticker) that increases the relaxation time by a factor 5:$\tau_{21} \simeq 5\tau_{18}$) as shown in Fig.16.

To summarize the experimental results, three experimental facts present strong analogies with the fracture of brittle solids: rupture suddenly appears within the linear regime, it is driven by the tensile stress and it exhibits a parabolic profile in the extensional test. Moreover, the critical rupture stress $\sigma_f \approx 0.5Y$ and is independent on the bonding energy ϵ.

5.2. *The Griffith-Pomeau theory*

Solid mechanics predicts that tensile rupture of solids occurs for an applied stress high enough to break atomic bonds. However the true values of critical stress are several orders of magnitude lower than the predicted value. Griffith[32)] clarified this

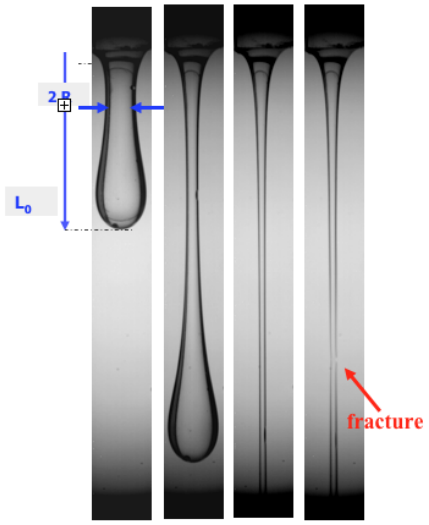

Fig. 13. Flow and fracture of a pendant drop.

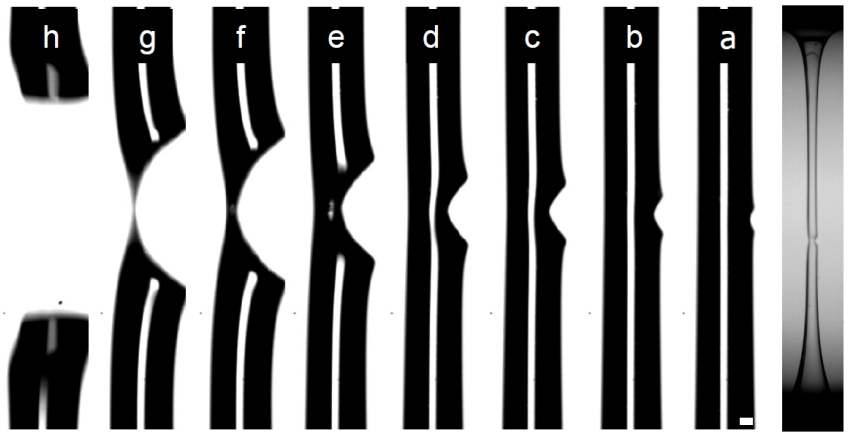

Fig. 14. Pictures of the propagation of the fracture across the sample $r = 6$from the right to the left. The time left to pinch off corresponding to each picture labelled with a letter is: a (8.50 ms), b (5.16 ms), c (2.67 ms), d (2.00 ms), e (1.00 ms), f (0.33 ms), g (0.17 ms) and for h (0.33 ms after the pinch off). The last picture on the right shows almost all the elongated drop the crack being well developed. The white scale bar corresponds to 0.1 mm.

discrepancy and laid down the foundation of brittle fracture theory: microcracks created during material processing act as stress concentrators and lower the overall strength. The Griffith's point of view starts up with preexisting micro-cracks and considers the energy required for them to grow spontaneously under a given constant stress. A surface energy has to be paid to break more cohesive bonds, counterbalanced by the bulk elastic energy released by the opening of the crack. For a given stress σ_N the Griffith energy cost W for a crack of size l reads then:

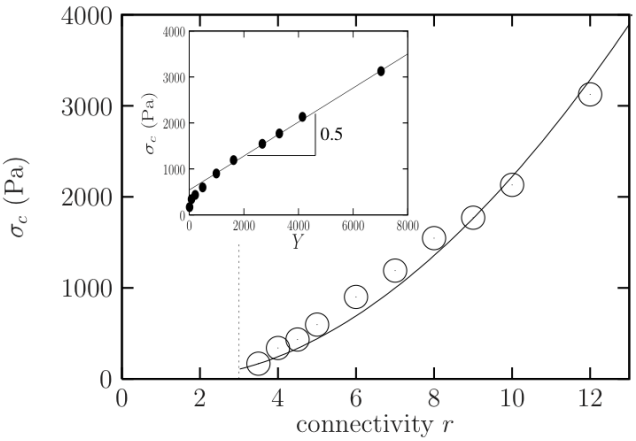

Fig. 15. Plot of the rupture stress coming from the pendant drop experiments (circles) and expected values from Eq. 5·6 as a function of the connectivity r. f as been fixed to its expected value : $f = 0.5$. The only free parameter is then α. Here, $\alpha = 0.9$ ($\alpha \sim 1$ as expected). The vertical dashed line corresponds to the percolation threshold (r=3). The inset gives the variation of the experimental rupture stress with the Young modulus $Y = 3\mu_0$, corresponding to the different connectivites. Note that the observed deviation of σ_c from its linear dependance with Y observed at small r, originates form the vicinity of the percolation threshold.

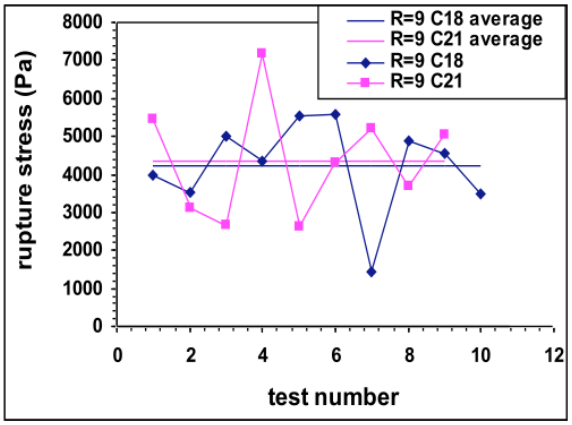

Fig. 16. Statistics of the rupture stress for pendant drop experiments with two series of samples with the same surfactant concentration $\phi = 10\%$ and same connectivity $r = 9$ but with two different lengths for the hydrophobic stickers (21 versus 18 methyl groups)

$$W(\sigma, l) = \frac{\pi}{2} l^2 \gamma - \alpha \frac{\pi l^3 \sigma^2}{6Y}, \tag{5·1}$$

with l the size of a disc-like crack, γ the cohesive energy per unit area, $Y = 3\mu_0$ is the Young modulus and $\alpha \simeq 1$ a constant depending on geometrical factors. Note that Grffith's therory is based on the hypothesis that the deformation of the material is in the linear elastic regime, i/e. $\sigma \propto Y\Delta V/V$. The variation of $W(\sigma, l)$ with l for a fixed σ is plotted in Fig. 17. It has typical shape of the free energy for a nucleation

phenomenon.

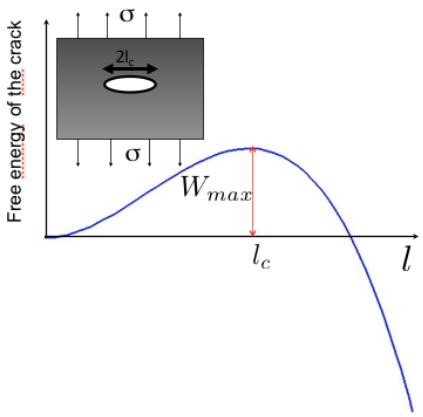

Fig. 17. Variation free energy of a crack with its length (Eq. 5·1)

The stress σ being fixed, $W(\sigma, l)$ reaches a maximum:

$$W_{max}(\sigma) = \frac{2\pi}{3\alpha^2}\frac{\gamma^3 Y^2}{\sigma^4} \tag{5·2}$$

for a crack size (the so called Griffith length)

$$l_c(\sigma) = \frac{2}{\alpha}\frac{\gamma Y}{\sigma^2} \tag{5·3}$$

For a crack of size larger than $l_c, dW/d\sigma < 0$, leading to a catastrophic growth of the crack, in contrast with a crack of size smaller than l_c. In brittle solids, micro-cracks are formed irreversibly during the material processing. Upon increasing the applied stress the largest amongst them become critical and leads to fracture. In our case however, the elastic network results from an equilibrium self assembly and micro-cracks can only arise from thermally activated fluctuations of the connectivity. Indeed, in the absence of applied stress, there is a statistical thermal distribution of domains without polymers connecting droplets $n(l) \propto e^{-4\pi\gamma l^2/kT}$ that we *identify* with microcracks. Pomeau[33] suggested that the Griffith's energy (Eq. 5·1) can be viewed as an energy barrier of height $W_{max}(\sigma)$ that can be overcome by thermal fluctuations according to Kramers theory. This occurs as soon as $W_{max}(\sigma_c) \leq k_B T$. Then, from Eq. 5·2, a fracture appears for $\sigma \leq \sigma_c$ with

$$\sigma_c = \left(\frac{2\pi}{3\alpha^2}\frac{\gamma^3 Y^2}{k_B T}\right)^{1/4}. \tag{5·4}$$

Notice that Griffith-Pomeau theory of thermally activated fracture failed to quantitatively explain thermally activated fracture nucleation in solids[34] until yet, because in through solids, thermal fluctuations are *irreversible*, in contrast with the present material where healing and growth of the microcracks are both possible.

We need a precise estimate of the surface energy γ. The micro-cracks appear well before the fracture forms an interface with air. A micro-crack corresponds to a surface across which there is no connection between oil droplets. The crack is completely wet by the aqueous solvent and the only contribution to γ comes from the polymer network.

5.3. *Entropic origin of the wet fracture interfacial energy*

At first sight, the nucleation of crack requires some stickers to be pulled out of the oil droplets and dangle free into the solvent. This would cost a free energy per link equal to the sticking energy ϵ. The corresponding fraction surface energy γ would be then proportional to this binding energy, and consequently (see Eq.5·4), the critical fracture stress σ_c would increase with ϵ. This is not was is observed as shown clearly in Fig.16. But in fact a crack can be achieved at a much lower energy cost corresponding to the lack of accessible configurations of the polymers which face the crack surface. These cracks always exist, in the fluid, due to equilibrium thermal fluctuations. A micro-crack corresponds to a region without polymers connecting droplets. In the vicinity of a crack, polymers do not cross the crack surface and therefore lose roughly half of the configurations they would have had if they were far from the crack surface, Fig. 1. Those polymers are redistributed parallel to the crack surface (see Fig. 18).

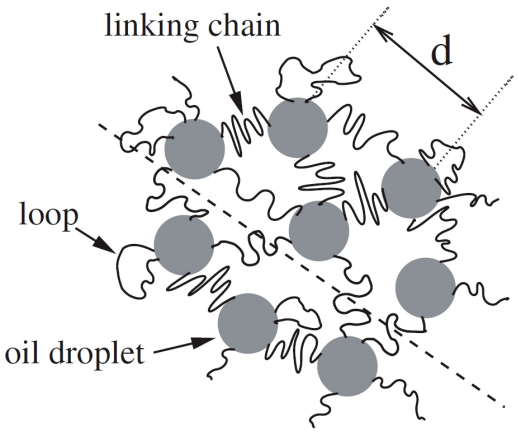

Fig. 18. (Left) Before the crack nucleation (bold dashed line) polymers can bridge oil droplets on both side of the bold dashed line. (Right) When the crack occurs, the same polymers can not cross the bold dashed line anymore and form bridges in the other directions.

So the free energy cost associated to the crack is $kT \ln 2$ per active polymer. Therefore the surface energy can be written as

$$\gamma = \frac{fr}{2d^2} kT \ln 2 \tag{5·5}$$

where r is the average number of hydrophobic stickers per droplet (connectivity), f is the average fraction of bridging configurations for a given polymer ($f \sim 0.5$[18]). d is the center-to-center distance between droplets $d = (4\pi/3/\phi)^{1/3} r_0$ (ϕ and r_0 are

the volume fraction and the oil droplet radius respectively. The typical value of γ is extremely low and roughly equal to 10 $\mu J.m^{-2}$. This a depletion interfacial tension of purely entropic origin. Knowing the surface energy γ we are able to calculate the critical stress σ_c (Eq. 5·4), above which the fracture occurs:

$$\sigma_c = \left(\frac{3}{\pi\alpha^2} \left(\frac{f \ln 2}{4} \right)^3 \phi^2 \frac{r^3}{r_0^6} \right)^{1/4} (kTY)^{1/2} \tag{5·6}$$

Since far from the percolation threshold the Young modulus is roughly equal to $Y = 3nk_BT$ where $n = 3\phi rf/(4\pi r_0^3)$, we eliminate ϕ and r_0 in Eq.5·6 which can then can be approximated by:

$$\sigma_c \simeq \left(\left(\frac{\ln 2}{3} \right)^3 \frac{\pi}{4\alpha^2} rf \right)^{1/4} Y \tag{5·7}$$

For typical values of f and r, the prefactor in remains of the order of unity: $\sigma_c \sim Y$ (far from the percolation threshold). Fig.15 shows that the critical stresses measured during the pendant drop experiment are in very good agreement with the ones derived from our simple approach (Eq. 5·7), when the polymer concentration changes (r increases), at a fixed volume fraction of droplets. This result confirms the physical basis of the fracture interfacial energy we have chosen. The fracture mechanism of the transient network is a two step process. Tthe first step consists in the spontaneous nucleation of a wet fracture starting up from a lack of cohesion of the network, the microcrack being filled up with solvent. The second step corresponds to the destabilsation of the capillary bridge, driving eventually to the dry fracture with parabolic profile as displayed in Fig.14. This last step and the properties of the fracture propagation will be described in details in the next section.

§6. Propagation of a brittle fracture in the transient network[24)]

6.1. *Velocity of the fracture propagation in an elastic solid*

In an elastic solid the velocity of fracture propagation is high, with a maximum given by the sound velocity $v_{max} \approx (Y/\rho)^{1/2}$.

This result can be shown using the following oversimplified argument.[35)] In a 2D version of the Griffiths theory, the Griifith energy cost for a crack of size l can be written as a function of the Griffith length $\Delta E = 2\gamma l - \pi l^2\sigma^2/Y = 2\gamma l_c - 2\gamma(l-l_c)^2/l_c$, which is valid for $l < l_c$. For $l > l_c$, the material fails suddenly and the fracture propagates so rapidly that the total energy of the 2D solid can be considered as constant with time: $\Delta E_{tot} = 2\gamma l_c = 2\gamma l_c - 2\gamma(l - l_c)^2/l_c + E_{kin}$. Indeed, there is an extra term in the total energy : the kinetics energy of the atoms located in the region (of size l^2); where the constraint is relaxing. $E_{kin} \approx \rho l^2 (du/dt)^2$ where ρ is the density of the material, and u is the displacement of the atoms caused by the relaxation of the stress inside a region of size l where the fracture takes place. So $u \approx l\sigma/Y$ and $E_{kin} \approx \rho l^2(\sigma^2/Y^2)v^2$ where $v = dl/dt$ is the fracture velocity. Now, because all the released elastic energy is converted into kinetics energy, one finds: $v = v_{max}(1 - l/l_c)$.

We will se that in the transient network under consideration, the velocity of the fracture is much smaller than the sound velocity, despite the fact that the fracture propagation can be considered as brittle.

6.2. *Experimental results*

During the pendant drop experiment, a filament is formed from the drop which hangs at the outlet of the glass tube. As the drop falls, this filament continuously thins up and the tensile stress steadily increasing, until a crack nucleates at the surface of the filament for a critical stress $\sigma_c \simeq 0.5Y$.[14] Then the fracture propagates across the sample and eventually leads to the rupture of the drop (fig. 14). In the experiments presented here, the fracture mechanism is a two step process. the first step consists in a spontaneous nucleation (thermally activated crack) of a microcrack within the oil droplet/telechelic polymers network, the microcrack being filled up with solvent. In the following we discuss in details the second step which corresponds to the destabilization of the capillary bridges and the propagation of a dry fracture which propagates through the material.

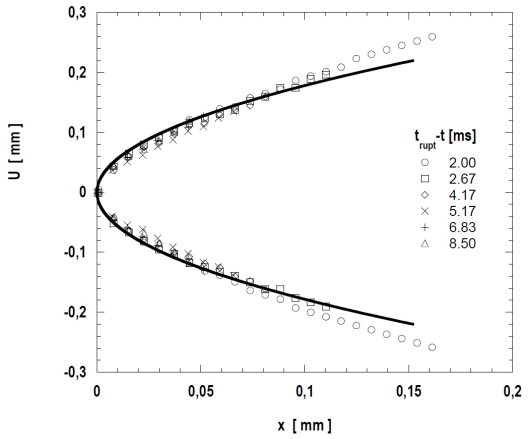

Fig. 19. Fracture profiles $u(x)$ for different times before the pinch off, in the fracture moving frame, corresponding to the pictures of the part a of this figure. The black line is a parabolic fit corresponding to the eq. (6·1) with $G = 2\gamma_s$. We report only the profile for $L < 0.1D_0$.

It's worth noting that from the beginning of the propagation up to the pinch-off (i.e., the sample is separated in two parts) the fracture profile exhibits a parabolic shape (Fig. 19) expected for an elastic solid breaking under tension[31].[30]

$$u(x) = \frac{K_I}{Y'}\sqrt{\frac{8x}{\pi}} \tag{6·1}$$

where $Y' = Y/(1-\nu^2)$ due to the plane strain condition.These observations were confirmed by a quantitative analysis of the fracture profile $u(x)$ on the overall crack propagation across the sample. Different fracture profiles measured in the fracture moving frame and a parabolic fit are represented in figure 14. The (local) stress intensity factor K_I is thus estimated using equation (6·1) and the corresponding strain energy release rate G is evaluated according to the equivalence:

$$G = \frac{K_I^2}{Y'} \tag{6·2}$$

We stress the point that the use of equation (6·1) essentially assumes a 2D symmetry of the crack profile which is not realistic in the case of a cylindrical filament. However, since the movie has been selected in order to present an excellent orthogonality between the camera orientation and the direction of crack propagation, the observed opening profile provides a good estimate of the local stress intensity factor, the measurement being more accurate for shorter cracks.

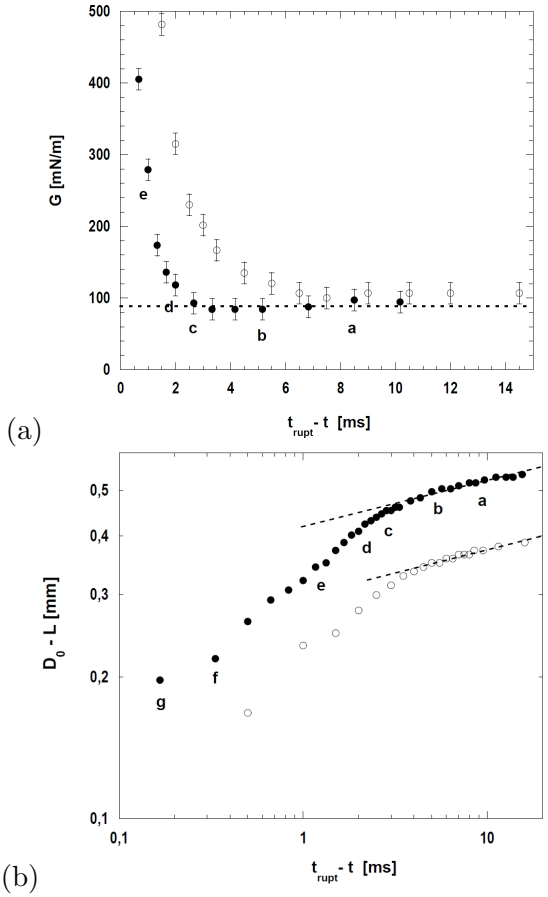

Fig. 20. (a) Fracture energy versus the time which left to pinch-off $t_{rupt} - t$ for $r = 6$ (closed circles) and$r = 12$ (opened circles) fluids. The letters still correspond to the picture in fig. 14 associated with the $r = 6$ fluid fracture. The dotted line corresponds to $G = 2\gamma_s$. (b) Evolution of the total length of the fracture L ($D_0 - L$ in the graph) with the time which left to pinch-off $t_{rupt} - t$. The legend is the same as part a. The diameter of the filament when the crack occurs at the surface of the material D_0 are equal to 0.584 mm and 0.407 mm for ($r = 6$) and$r = 12$) fluid respectively. The dotted lines correspond to the linear fit of the data which give roughly a crack speed $V = 4$ mm/s.

The variation of the estimated fracture energy G and the measured length of fracture L as a function of $t_{rupt} - t$ are represented in figure 20. Two distinct regimes

are clearly evidenced depending on the length of the crack:

(i) for $L < 0.1D_0$, both the fracture energy and the crack speed remain almost constant with values roughly equal to $G \approx 100\ \mathrm{mJ/m^2}$ and $V = 4\ \mathrm{mm/s}$. It turns out that the estimated value for G is roughly twice the surface tension $\gamma_s \simeq 50\ \mathrm{mJ/m^2}$ of the stabilized oil-in-water droplet microemulsion without telechelic polymers (that we will call the solvent). We remark firstly that the surface energy needed to pull-out the hydrophobic stickers from the oil droplet γ_{pol}, of the order of $10\mu\mathrm{N/m}$[14] is completely negligible. Secondly, the relation $G \approx 2\gamma_s$ suggests that there is no significant dissipative contribution in the crack tip region.

(ii) for $L > 0.1D_0$, the estimated fracture energy and the crack speed increase when we go closer to the pinch-off. It's worth noting that the results concerning G must be interpreted with caution as finite size effect may be important. It is then questionable whether the use of equation (6·1) to fit the profile is still justified. Moreover, in this regime we clearly observe an axisymmetric thinning of the filament rather than a fracture which grows and propagates across the sample (images d-g in fig.14). This was confirmed by the analysis of the variation of the diameter of the filament.

6.3. *Trumpet model for the fracture in a Maxwell fluid*

In order to provide a rationale for the presented behaviour, we review here the de Gennes model of the viscoelastic trumpet[36),37)] reassessed by Saulnier et al,[38)] which present a qualitative theroretical analysis of the dissipative process during the bulk fracture in a viscoelastic material; we apply this scaling approach to the simplest case of a Maxwell fluid.[38)] This model allows to explain at the level of scaling law the remarkable relation between the fracture energy per unit area $G(V)$ at crack velocity V and G_0, the limiting value of the fracture energy at zero rate crack that was reported for elastomeric materials:[39),40)]

$$G(V) = G_0(1 + \phi(a_T V)) \tag{6·3}$$

where a_T is the temperature shift factor given by the Williams-Landel-Ferry equation.[41)] For a Maxwell fluid, the complex modulus $\mu(\omega)$ as function of frequency is the following:

$$\mu(\omega) = \mu'(\omega) + i\mu''(\omega) = \mu_0 \frac{i\omega\tau}{1 + i\omega\tau} \tag{6·4}$$

A low frequency ($\omega\tau \ll 1$), the modulus is purely imaginary ($\mu = i\omega\mu_0\tau$) and the material behaves as a liquid of viscosity $\eta = \mu_0\tau$.

At high frequency ($\omega\tau \gg 1$) we are dealing with an elastic solid with an elastic moculus $\mu \approx \mu_0$. de Gennes discusses in[36)] the consequences of this property on a moving fracture. Let consider a fracture of crack lenght $L(t)$ moving at velocity V. He shows that for a viscoelastic medium, the scaling law for the stress σ as a function of distance r from the crack tip is still equivalent to that we have for a steadyly growing mode I interface in plane stress or plane strain in an elastic medium[43)]

$$\sigma(r) \cong \frac{K_I}{\sqrt{r}} \tag{6·5}$$

where K_I is the applied stress intensity factor. The key point of de Gennes theory is that far from the crack tip, $r > V\tau$, i.e. at large spatial scales or long time, viscous dissipation occurs and the dissipation $T\dot{S}$ (per unit length of the fracture line) is:

$$T\dot{S} = V(G(V) - G_0) = \int dxdy\sigma\dot{\gamma} \tag{6·6}$$

where σ is the local stress and $\dot{\gamma}$ the local share rate. During crack propagation, the strain rate imposed to the material is high near the fracture tip and lowers as the distance r to the head increases (far from the fracture tip the material has more time to relax the stress) and de Gennes assumes a simple scaling for the local sweeping frequency of the form $\omega \cong V/r$.

Since the complex strain γ can be related to the complex stress σ through the complex modulus $\gamma = \sigma/\mu(\omega)$ equations (6·4,6·6) lead for a Maxwell fluid to:[38)]

$$G(V) - G_0 = -K_I^2 \int_{\omega_{min}}^{\omega_{max}} \frac{\mu''(\omega)}{\mu'(\omega)^2 + \mu''(\omega)^2} \frac{d\omega}{\omega} = \tag{6·7}$$

$$= \frac{K_I^2}{\mu_0 \tau} \left(\frac{1}{\omega_{min}} - \frac{1}{\omega_{max}} \right) \tag{6·8}$$

The limiting values $\omega_{min} = V/L$ and $\omega_{max} = V/\ell$ define the range of frequency over which the material is excited, ℓ being the length of a small microscopic non linear zone (see figure 21).

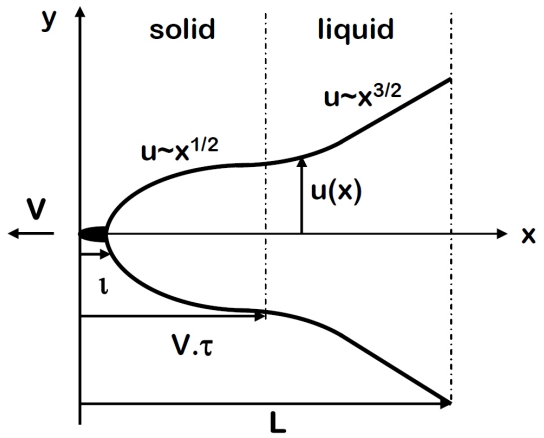

Fig. 21. Schematic representation of the space and time scales of associated to a crack of length L moving with a velocity V in a Maxwell fluid according to the trumpet model.[38)] A small microscopic non linear zone of length ℓ is represented in black. The behavior of the material is solid like at scales smaller than $V\tau$, then fluid like at larger scales.

For a simple Maxwell fluid exhibiting a crack propagation we can distinguish three spatial regions with different viscoelastic properties corresponding to three regimes of frequencies:

(i) $0 < x < \ell$: directly ahead the crack tip there is a small microscopic non linear zone of length ℓ, independant of the separation rate, where the fracture process lead to the G_0 term of the fracture energy in equation (6·3); ℓ is typically on the order of 100 $\mathring{A}$.[38)]

(ii) $\ell < x < V\tau$. In this region, the complex modulus is essentially real ($\mu(\omega) \approx \mu_0$), the viscous dissipation is negligible and the material can be considered as an elastic solid.

(iii) $V\tau < x < L(t)$ In this region, the complex modulus is essentially imaginary ($\mu(\omega) \approx i\omega\mu_0\tau$) and the material can be viewed as Newtonian liquid of viscosity $\eta = \mu_0\tau$. Only this region contributes to the viscous dissipation processes.

From this model several interesting features appear:

(i) The limiting value G_0 of the fracture energy at zero rate which characterizes also the relevant energy of the fracture is governed by the small non linear zone of size ℓ near the crack tip and $G_0 = 2\gamma_s$ is the Dupr work needed to cut the material in air, γ_s being the surface tension of the material.

(ii) If the fracture length is small ($\ell < L(t) < V\tau$), viscous dissipation does not occur according to equation (6·7) and $G(V) = G_0$; this regime takes place at short times or if there is some maximal cut-off for the length fracture $L_{max} < V\tau$, as it does for the filament rupture experiment reported in this paper, where $L_{max} = D_0 \approx 600$ μm is the diameter size of the filament just before failure. In this purely elastic regime of the fracture propagation, where the viscous region does not appear because of the finite size of the sample, the profile $u(x)$ of the fracture should be parabolic[43)] as in equation (6·1), and it should not depend on the rate of propagation of the fracture.
(iii) Viscous dissipation will occur only if $L_{max} > V\tau$. In this regime, equations (6·7,6·2) give:

$$\frac{G(V, L(t))}{G_0} = 1 + \frac{L(t)}{V\tau} \tag{6·9}$$

provided that ℓ remains small with respect to the sample dimension. In this zone ($V\tau < x < L(t)$), de Gennes has shown that the scaling form (6·5) for the stress components remains valid for a viscoelastic medium leading to the expected profile $u(x) \sim x^{3/2}$. The sign change in the concavity of the fracture profile at $x \sim V\tau$ is at the origin of the name "trumpet" for this model. Such a trumpet profile has been experimentally observed for adhesive fractures in polymer melts.[38)] We remark that the scaling form (6·3) can not be observed in the fracture of Maxwell fluids since they do not present an elastic behaviour at long time scales as is the case of viscoelastic solids that was initially considered by de Gennes.[37)]

6.4. *Application of the Trumpet model to the experiments*

For our fluids ($r = 6$)and ($r = 12$) the characteristic length $V\tau$ is respectively 2.4 mm and 8 mm, which are always larger than the upper bound for the crack length $D_0 = 0.6$ mm, the diameter of the filament when the crack appears. Therefore the response of the material is completely elastic ($L < V\tau$), the size of the sample being too small to see any viscous dissipation on the overall rupture phenomenon. The fracture energy is thus expected to be independent of crack speed and to equal

$G_0 = 2(\gamma_s + \gamma_{pol})$. The first term is the classical Dupr work needed two form two new air/gel surfaces (dry fracture). However before dry fracture occurs by instability of the capillary bridge, the wet fracture must have already occurred and its interfacial cost is $2\gamma_{pol}$. As reported by Tbuteau et al.,[14] this term of purely entropic origin is related to the loss of configurational entropy of polymer chains at the crack surface $\gamma_{pol} \simeq (\ln 2/2) k_B T N_P^{2/3}$, where $N_P \approx 3\phi r/8\pi b^3$ is the number density of polymer chains in the sample (cf. Fig. 18). This interfacial tension is extremly low and roughly equal to 10 μNm^{-1} and is thus negligible compared to the air/gel interfacial tension $\gamma_s \simeq 50$ mNm^{-1}. It has been proved that for many systems G_0 exhibits a marked dependence on V, and most of the rate dependence of $G(V)$ then originates from the rate dependence of G_0 itself.[42] Raphael and de Gennes[44] have shown theoretically that the surface energy required to debond the connectors between two surfaces is indeed velocity dependant. However, in our fluid this argument would apply to the component γ_{pol} which is negligible in front of the dominant term γ_s, thus resulting in a substantial independence of G_0 from V. Although the condition $L < V\tau$ is respected throughout the experiment, the trumpet model can only accurately describe the first observed regime of crack propagation where $L < 0.1D_0$. This is not surprising, since the modelling is relative to the fracture propagation in a semi-infinite medium. The second regime for $L > 0.1D_0$ must clearly be attributed to the finite size of the soft filament and to the increasing value of the strain in the progressively thinning ligament (cf. Fig. 14). In the regime 2, $(L > 0.1D_0)$, we invoke finite size effects but it's possible that we observe a blunting phenomenon. Indeed, in this regime the deformation of the polymers is not linear. A secondary contribution is the progressive failure of the rough 2D approximation. The modeling of this second regime certainly requires further analysis.

6.5. *Microscopic model for the fracture velocity*

In the following we will only focus on the first elastic regime where both G and V are constant in time and also take approximately the same values in the two fluids $r = 6$ and $r = 12$, although Y and K_I are significantly different. It's worth noting that $V \ll C$, C (of the order of 1 m/s) being the speed of sound in the medium. What is the mechanism that explains this low speed propagation?

Basically, we argue that the scaling of the velocity V of the fracture is given by the characteristic speed of relaxation of a microemulsion droplet at the opening crack interface, under the action of the unbalanced elastic force of the polymer bridge towards the gel (fig. 22). This velocity is given by balancing the elastic force and the viscous drag force acting on the droplet (Reynolds number $R_e \ll 1$). The control of the crack velocity by network /solvent friction has been already proposed by Baumberger *et al.*[45),46)] in the *viscoplastic* fracture dynamics of an other class of reversible gel, i.e. gelatin.

$$6\pi\eta_w b V \sim Y d_0^2 \tag{6·10}$$

where $d_0 \simeq (4\pi\phi/3)^{1/3} b$ is the mean distance between two connected beads and η_W is the viscosity of the water. A more precise calculation developedjust bellow gives:

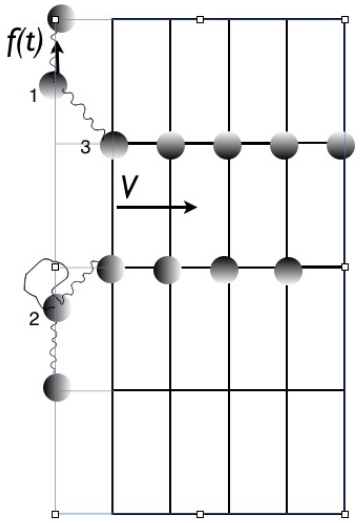

Fig. 22. Cartoon of the viscous relaxation mechanism of a bead at the tip of the fracture. The polymer bridge between beads (1) and (2) just debonded, forming a loop on bead (2). Bead (1) thus experiences the srpingback force $f(t)$ due to the gel under tension; this will lead to an increasing extra tension on bead (3) and crack propagation at velocity V.

$$V < \alpha \frac{Y d_0^2}{6\pi\eta_W b} \tag{6·11}$$

For the ($r = 12$) sample inequality (6·11) gives $V < \alpha 25$ mm/s ~ 6 mm/s for a reasonable expected value $\alpha \sim 0.25$.

Just before the bead at the tip of the fracture is released (at time $t = 0$) by the debonding of a polymer bridge, it is submitted to the normal force :

$$f_0 = \sigma_i (d_0/\sqrt{\lambda_i})^2 = \frac{\sigma_i d_0^2}{\lambda_i}, \tag{6·12}$$

where $\lambda_i = d_i/d_0$ is the elongation of the network at the crack tip, d_0 is the mean distance between droplets at rest and σ_i is the local normal stress at the tip of the fracture. Note that equation (6·12) assumes the incompressibility of the gel. For $t > 0$, the bead experiences the following springback force due to the gel under tension (fig.22):

$$f(t) = \frac{\sigma(t) d_0^2}{\lambda(t)} \tag{6·13}$$

From the relationship between $\sigma(t)$ and $\lambda(t) = d(t)/d_0$ given by the affine network model of the unentangled rubber elasticity theory,[27] one gets:

$$f(t) = \frac{Y d_0^2}{3} \left(\lambda(t) - \frac{1}{\lambda^2(t)} \right) \tag{6·14}$$

The size of the bead is submicrometric and so, its motion in water obeys the Stokes law:

$$6\pi\eta_W b d_0 \frac{d\lambda}{dt} = f(t) \tag{6·15}$$

where η_W is the viscosity of the water. Substituting (6·14) in (6·15) and integrating the obtained differential equation with the initial condition given by (6·12) gives:

$$\lambda(t) = \left[1 + (\lambda_i^3 - 1)\exp(-t/\tau_1)\right]^{1/3} \tag{6·16}$$

with a characteristic time

$$\tau_1 = \frac{6\pi\eta_W R}{Y d_0} \tag{6·17}$$

To obtain the characteristic fracture velocity, one can estimate that the next bead will debond (causing the growth of the fracture of length d_0/λ_i) when $\lambda = f_d\lambda_i$, where $\lambda_i^{-1} \leq f_d \leq 1$ is a critical elongation felt by the chain on the next bonded bead, that is difficult to estimate. Indeed, the relaxation of the debonded bead induces extra elastic tensions on the next bead at the tip of the fracture that will grow with time. The time necessary to reach this critical elongation is then according to eq. (6·16):

$$t_p = \tau_1 \ln\left[\frac{\lambda_i^3}{f_d\lambda_i^3 - 1}\right] \tag{6·18}$$

The time scale is thus given by eq. (6·18) with logarithmic corrections. Finally the fracture velocity is:

$$V \equiv \frac{d_0}{\sqrt{\lambda_i}}\frac{1}{t_p} = \frac{Y d_0^2}{6\pi\eta_W b}\left[\sqrt{\lambda_i}\ln\left(\frac{\lambda_i^3 - 1}{f_d^3\lambda_i^3 - 1}\right)\right]^{-1} \tag{6·19}$$

The function $g : \lambda_i \rightarrow \left[\sqrt{\lambda_i}\ln\left(\frac{\lambda_i^3-1}{f_d^3\lambda_i^3-1}\right)\right]^{-1}$ exhibits a maximum whose position and value depend on f_d and determines an upper bound for the fracture velocity. We choose $f_d = 0.5$, Indeed $2 < \lambda_i < 8$ ($\lambda_i = 2$ corresponds roughly to the maximal macroscopic elongation for the network experimentally observed before rupture % occurs in pendant drop experiments and $\lambda_i =\sim 18$[47)] corresponds to the maximal elongation usually observed in permanent rubbers), one gets $\max(g) = \alpha = 0.25$. We note that $\max(g)$ is a decreasing function of f_d. So the choice $f_d = 0.5$ will give the upper limit for the estimation of the crack velocity.

The debonding of a polymer bridge under tension leads to a viscous dissipation due both to the motion of the released bead in the solvent and to the friction of the monomer of the polymer bridge with the solvent too. Both forms of dissipated energy will be of the same order of magnitude. the polymer contribution being even smaller since the hydrodynamic radius of the polymer chain $R_H \sim 4nm < b$.

We focus here to the viscous dissipation due to the motion of a released bead.The energy dissipated by a bead after debonding is given by:

$$E_d = -\int_{\lambda_i}^{1} f(t) d_0 d\lambda \tag{6·20}$$

where $f(t)$ is given by equation (6·14). This leads to a dissipative contribution to the fracture energy ΔG_0:

$$\Delta G_0(V) \approx (N_p/2)^{2/3} \frac{Y d_0^3}{2} = \frac{1}{3}(\pi/12)^{1/3} \frac{r^{2/3} b Y}{\phi^{1/3}} \tag{6·21}$$

where we have assumed that roughly half of the polymer chains are in bridge configuration[18] and that $\lambda_i = 2$. For the fluid ($\phi = 10\%$, $r = 12$), $\Delta G_0(V) \sim 35$ $\mu \mathrm{Jm}^{-2} \ll 2\gamma_s$, which is once again of the same order as γ_{pol} and is thus negligible in front of the dominant term $2\gamma_s$.

Acknowledgements

A large part of the work described in thi slecture notes was realized by many collaborators: Jacqueline Appell, Matteo Ciccotti, Serge Mora, Grégoire Porte, Hervé Tabuteau. I thank all of them. This work was supported in part by ANR under contact ANR-06-BLAN-0097 (TASNET).

References

1) Zilman, A.G., Safran S. A., *Europhys. Lett.* **63** 139 (2003)
2) Semenov, A.N., J.F. Joanny, and A.R. Khokhlov *Macromolecules* **28** 1066 (1995).
3) Annable, T., R. Buscall, R. Ettelaie, and D. Whittlestone, *J. Rheology* **37** 695 (1993).
4) Lee J. H., Gustin J. P., Chen T. H., Payne G. F. and Raghavan S. R. *Langmuir 2005* 2005 **21** 26
5) Zhu, C., J.H. Lee, S.R. Raghavan, and G.F. Payne,*Langmuir* **22** 2951 (2006).
6) Warriner H. E., Davidson P., Slack N. L., Schellhorn M., Eiselt P., Idziak S. H. J., Schmidt H. W., Safinya C.
7) Ramos L., Ligoure C. *Macromolecules* **40** 1248 (2007)
8) Lodge T. P., Taribagil R., Yoshida T., Hillmyer M. A. *Macromolecules* 2007 **40** 4728
9) Nakaya-Yaegashi K., Ramos L., Tabuteau H., Ligoure C. *J. Rheol.* 1993 **52** 359
10) Appell J., Porte G., Rawiso M. *Langmuir* 1998 **14** 4409
11) M. Filali, R. Aznar, M. Svenson, G. Porte and J. Appell, *J. Phys. Chem. B* **103**, 7293 (1999)
12) Bagger-Jõrgensen H;, Coppola L., Thuresson K., Olsson U. and Mortensen K. *Langmuir* **13** 4204 (1997)
13) Filali, M., Ouazzani M. J., Michel E., Aznar, G. Porte and J. Appell, *J. Phys. Chem. B* **105** 10528 (2001)
14) Tabuteau, H., Mora, S., Porte G., Abkarian M. and Ligoure C. *Phys. Rev. Lett.* **102** 155501 (2009)
15) G. Porte, , C. Ligoure , J Appell R. Aznar, *J.Stat. Mechanics : theory and experiments* P05005 (2006)
16) de Gennes P. G. *Rep. Prog. Phys.* **32** 187 (1969)
17) B. V. Derjaguin, *Kolloid. Zeits.* **69**, 155 (1934)
18) Testard V., Oberdisse J. and Ligoure C. *Macromolecules* **41**, 7219 (2008)
19) Zilman A., Kieffer J., Molino F., Porte G. And Safran S. A. *Phys. Rev. Lett* **91** 015901 (2003)
20) Hurtado, P., Berthier L. and Kob W. *Phys. Rev. Lett.* **(98** 135503 (2007)
21) Sprakel J., Besseling N. A. m;, Cohen-Stuart M. A., Leemarkers F; A. M. *Eur. Phys. J. E* **25** 163 (2008)

22) Pham, Q. T., Russel W. B., Thibeault J. C., Lau W. *Macromolecules* **32** 2996 (1999)
23) François J., Beaudoin E., Borisov O. *Langmuir* **19** 1011 (2003)
24) Tabuteau H., Mora S., Ciccotti M. and Ligoure C. *submitted to SoftMatter*
25) Green M. S. and Tobolsky A. V.. *J. Chem. Phys.* **14** 80 (1946)
26) Tanaka F; and Edwards S. F. *Macromolecules* 1992 **25** 1516
27) Rubinstein M. and Colby R. H. *Polymer Physics* Oxford University Press, New-York (2003)
28) Michel E., Filali M., Aznar R., Porte G. and AppellJ. *Langmuir* **16** 8702 (2000)
29) Stauffer D. *Introduction to percolation theory* Taylor Francis, London (1985)
30) Barenblatt G. 1962 *Adv. Apll. Mech.***7** 55
31) Greenwood J. and Johnson K. 1991 *Phillos. Mag.* **43** 697
32) Griffith A. *Phil. Trans. R. Soc. A* 1921 **221** 163
33) Pomeau Y. *C.R. Acad. Sci. Ser. II* 1992 **314** 1992
34) Vannel L., Ciliberto S., Corte P-P., and Santucci S. *J. Phys. D: Appl. Phys.* 2009 **42** 214007
35) P. Oswald *Rhéophysique, Ou comment coule la matière* Belin Collection Echelles (2005)
36) de Gennes P-G., *CR Acad. Sci. Paris Srie II*1988 **307** 1949
37) de Gennes P-G. *Langmuir* 1996 **12** 4497
38) Saulnier F., Ondaruhu T., and Aradian A. and E. Raphaël , *Macromolecules* 2004 **37** 1067
39) Gent A. N and Shultz J. *J. Adhes.* 1972 **3** 281
40) Andrews E. H. and Kinloch A. *J. Proc. R. Soc. (London) 1973* **401** A332
41) Williams M. L., Landel R. F., Ferry J. D.. Am. Chem. Soc. 1995 **77** 3701
42) Gent A. N. *Langmuir* 1996 **12** 4492
43) Rice J. *in Fracture II and Advanced Treatise* LiebowitzH., ED 1968 Academic Press: New-York
44) Raphaël E. and de Gennes P-G. *J. Phys. Chem.* 1992 **96** 4002
45) Baumberger T., Caroli C. and Martina D. *Nat. Mat* 2006 **5** 552
46) Baumberger T., Caroli C. and Martina D. *Eur. Phys. J. E* 2006 **21** 81
47) Treloar L. R. G. *The physics of rubber elasticity 3rd edition* 1975 Clarendon Press, Oxford